American College of Neuropsychopharmacology

www.nature.com/npp

ARTICLE OPEN

Check for updates

The psychoactive cannabinoid THC inhibits peripheral nociceptors by targeting $Na_V1.7$ and $Na_V1.8$ nociceptive sodium channels

Yossef Maatuf[1], Ariel Iskimov[1], Alexander M. Binshtok[2,3]✉ and Avi Priel[1]✉

Δ^9-Tetrahydrocannabinol (THC), the primary psychoactive compound in cannabis, is widely recognized for its central effects mediated by cannabinoid receptors. Here, we uncover a distinct peripheral mechanism by which THC inhibits the excitability of nociceptive neurons. We show that THC directly targets the nociceptive voltage-gated sodium channels $Na_V1.7$ and $Na_V1.8$ through the conserved local anesthetic binding site. This interaction reduces sodium currents and suppresses action potential generation in peripheral sensory neurons. Our findings demonstrate that, beyond its central psychoactivity, THC exerts direct peripheral nociceptor inhibition via modulation of $Na_V1.7$ and $Na_V1.8$, offering new insight into cannabinoid-based analgesia independent of cannabinoid receptor signaling.

Neuropsychopharmacology (2026) 51:1091–1099; https://doi.org/10.1038/s41386-026-02355-9

INTRODUCTION

Cannabis has been used for centuries for its analgesic properties, and its clinical relevance in pain management continues to grow [1, 2]. The primary psychoactive constituent of Cannabis sativa, Δ^9-tetrahydrocannabinol (THC), produces central effects attributed mainly to its interaction with cannabinoid receptors, especially CB1, in the brain and spinal cord [3]. These receptor-mediated actions underlie much of the known psychoactive and analgesic activity of THC [4, 5]. However, recent studies have shown that non-psychoactive cannabinoids such as cannabidiol (CBD) and cannabigerol (CBG) modulate peripheral nociceptor activity by directly inhibiting voltage-gated sodium channels (Na_Vs), particularly $Na_V1.7$ and $Na_V1.8$ [6–11]. These channels, expressed in peripheral sensory neurons, play a central role in determining nociceptor excitability and are key targets for analgesic interventions, including local anesthetics that act via a conserved binding site [12–15]. While peripheral, receptor-independent mechanisms have been characterized for non-psychoactive cannabinoids, no direct peripheral mechanism of THC targeting either nociceptors or nociceptive Na_Vs has been previously established [16].

In this study, we identify a distinct peripheral mode of action for THC that is independent of cannabinoid receptor signaling. We show that THC directly interacts with $hNa_V1.7$ and $hNa_V1.8$ via the conserved local anesthetic binding site, leading to inhibition of sodium currents and suppression of action potential firing in nociceptive neurons. These findings reveal a previously unrecognized mechanism for THC-mediated peripheral analgesia and establish a non-canonical molecular pathway through which the psychoactive cannabinoid can inhibit nociceptor excitability and thereby pain.

MATERIALS AND METHODS

Animals

All animal procedures were carried out under protocols approved by the Hebrew University Ethics Committee (MD-20-16310-2 and HU-24-17640-1). Male and female Sprague–Dawley rat pups (Envigo, Jerusalem, Israel) at postnatal days 3–5 were used for neuronal isolations.

Neuronal primary cell cultures

Primary trigeminal (TG) neurons were acutely dissociated from 3–5-day-old Sprague–Dawley rats, as previously described [15]. Briefly, ganglia were collected from 2–4 pups and placed in ice-cold DPBS. The tissue was enzymatically digested at 37 °C using 0.025% collagenase P (Sigma-Aldrich, USA) for 10 min, followed by 0.25% trypsin (Gibco, USA) for 5 min. Neurons were mechanically dissociated by gentle trituration using fire-polished Pasteur pipettes of decreasing tip diameters, and undissociated tissue was removed. After centrifugation, the cell pellet was resuspended in Leibovitz's L-15 medium (Gibco, USA) supplemented with 10% fetal calf serum, 5 mM HEPES, 1% penicillin–streptomycin (Gibco, USA), and 100 ng/ml nerve growth factor (NGF; Alomone Labs, Israel). Cells were plated on glass coverslips coated with poly-D-lysine (PDL; Sigma-Aldrich, USA) and laminin (R&D Systems, USA) and incubated at 33 °C at room temperature. After 30 min, a complete L-15 medium was added, and cells were further incubated for 2–4 h at 33 °C in room air. Throughout this period, the neurons maintained healthy morphology and exhibited negative resting membrane potentials, as well as overshooting action potentials. No significant differences were observed in action potential or sodium current properties between cells used on the day of preparation and those stored at 4 °C for up to 48 h.

Molecular biology

The cDNAs encoding the human voltage-gated sodium channel α-subunits —SCN1A ($hNa_V1.1$; NM_001165963), SCN2A ($hNa_V1.2$; NM_021007), SCN3A

[1]The Institute for Drug Research, School of Pharmacy, Faculty of Medicine, The Hebrew University of Jerusalem, Jerusalem, Israel. [2]Department of Medical Neurobiology, Institute for Medical Research Israel-Canada, Faculty of Medicine, The Hebrew University of Jerusalem, Jerusalem, Israel. [3]The Edmond and Lily Safra Center for Brain Sciences, The Hebrew University of Jerusalem, Jerusalem, Israel. ✉email: alexander.binshtok@mail.huji.ac.il; avi.priel@mail.huji.ac.il

Received: 9 September 2025 Revised: 17 December 2025 Accepted: 11 January 2026
Published online: 21 January 2026

(hNa$_V$1.3; NM_001081677), SCN4A (hNa$_V$1.4; NM_000334), SCN5A (hNa$_V$1.5; NM_198056), SCN8A (hNa$_V$1.6; NM_014191), SCN9A (hNa$_V$1.7; NM_002977), and SCN10A (hNa$_V$1.8; NM_006514 each cloned into the pCMV6 expression vector, were obtained from Origene Technologies (USA). The sodium channel auxiliary subunit SCN1B (β1) cDNA was generously provided by Prof. Dr. Angelika Lampert (RWTH Aachen University, Aachen, Germany). The SCN3B (β3) auxiliary subunit cDNA was cloned from rat trigeminal ganglion (TG) neurons [15]. Site-directed mutagenesis of the hNa$_V$1.8 cDNA was performed using the QuikChange II XL Site-Directed Mutagenesis Kit (Agilent Technologies, USA).

Heterologous cell culture and channel expression

HEK293T and ND23/7 cells were cultured in DMEM (Gibco, USA) supplemented with 10% fetal bovine serum (Gibco, USA), 1% penicillin–streptomycin (Gibco, USA), and 25 mM HEPES (Gibco, USA) at 37 °C in a 5% CO_2 atmosphere. Transient expression of hNa$_V$1.1–hNa$_V$1.8 and mutant channel constructs was performed using Lipofectamine 3000 (Invitrogen, USA) according to the manufacturer's instructions. hNa$_V$1.1–hNa$_V$1.7 channels were co-transfected with the β1 auxiliary subunit, while hNa$_V$1.8 was co-transfected with the β3 subunit. At 24–48 h post-transfection, cells were transferred onto poly-D-lysine (PDL; Sigma-Aldrich, USA)-coated glass coverslips and used for whole-cell voltage-clamp recordings.

Chemicals

Δ^9-Tetrahydrocannabinol (THC) and Cannabidiol (CBD) were obtained from THC Pharm GmbH (Frankfurt, Germany) and prepared as stock solutions in ethanol (Carlo Erba, Italy) and DMSO (Sigma-Aldrich, USA), respectively. Cannabichromene (CBC) was purchased from Alomone Labs (Jerusalem, Israel), and Cannabigerol (CBG) was purchased from Symrise AG (Germany). Tetrodotoxin (TTX; Alomone Labs, Israel) was dissolved in molecular biology-grade water (Biological Industries, Israel). All stock solutions were stored at −20 °C until use and diluted in extracellular solution to achieve final working concentrations. To enhance drug solubility, Pluronic F-127 (20%) (Sigma-Aldrich, USA) was added to the final working solutions. The final concentrations of ethanol (≤1%), DMSO (≤1%), and Pluronic F-127 (0.01%) were confirmed not to affect action potentials or current properties. To isolate TTX-resistant (TTX-R) sodium currents, 100 nM TTX was included in the external and working solutions when recording from hNaV1.8 and mutant channels expressed in ND7/23 cells, as well as from TTX-R currents in trigeminal ganglion (TG) neurons.

Electrophysiology

Nociceptive neurons were identified based on a soma diameter of ≤25 µm and further verified by their responsiveness to capsaicin and the functional expression of Na$_V$1.7 and Na$_V$1.8 nociceptive sodium channels. Neurons with soma diameters >35 µm were classified as non-nociceptive. Whole-cell patch-clamp recordings were performed as previously described [17–19]. Patch pipettes were pulled from borosilicate glass capillaries using a P-1000 micropipette puller (Sutter Instrument, USA) and then fire-polished with an MF-900 microforge (Narishige, Japan) to achieve a resistance of 2–5 MΩ. Membrane currents and potentials were recorded using an Axopatch 200B amplifier (Molecular Devices, USA), digitized with a Digidata 1440 A interface, and acquired using pCLAMP 10.6 software (Molecular Devices, USA). Signals were sampled at 10 kHz and then low-pass filtered at 1 kHz. Recordings began at least 10 min after achieving whole-cell configuration to ensure current stability. The leak current was continuously monitored throughout the experiments. TG neurons with a leak above ~100 pA were discarded from the analysis. During recordings, extracellular solutions were continuously perfused using the ValveBank II perfusion system (AutoMate Scientific, USA). All experiments were conducted at room temperature.

Current-clamp recordings

Whole-cell current-clamp recordings of TG neurons were made with the fast current-clamp mode of the Axopatch 200B amplifier by using a pipette solution of (in mM): 130 K gluconate, 10 NaCl, 2 $MgCl_2$, 6 KCl, 14 Creatine phosphate, 4 MgATP, 0.3 GTP (Tris salt), and 10 HEPES, pH adjusted to 7.4 with KOH. The external solution contained (in mM): 145 NaCl, 5 KCl, 1 $MgCl_2$, 2 $CaCl_2$, 10 D-glucose, and 10 HEPES, with the pH adjusted to 7.4 with NaOH. Evoked action potentials were recorded using the current ramp protocol (300 pA in 0.5 s). The recorded membrane potentials were adjusted offline based on the calculated liquid junction potential of −15.5 mV.

Voltage-clamp recordings

Whole-cell voltage-clamp recordings were performed on TG neurons using an extracellular solution containing (in mM): 120 Choline-Cl, 30 NaCl, 10 TEA-Cl, 10 D-glucose, 1 $MgCl_2$, 1 $CaCl_2$, 0.02 $LaCl_3$, and 10 HEPES, adjusted to pH 7.4 with TEA-OH. The internal pipette solution contained (in mM): 61 CsF, 61 CsCl, 9 NaCl, 1.8 $MgCl_2$, 9 EGTA, 10 HEPES, 14 Creatine phosphate, 4 MgATP, and 0.3 GTP (Tris salt), adjusted to pH 7.2 with CsOH. Cesium and lanthanum were included to block voltage-gated potassium and calcium channels, respectively. For recordings in HEK293T or ND7/23 cells expressing Na$_V$ channels, the bath solution was (mM) 145 NaCl, 5 KCl, 1.8 $CaCl_2$, 1 $MgCl_2$, 10 D-Glucose and 10 HEPES (pH 7.4, NaOH), and the pipette solution (mM) 140 CsF, 10 NaCl, 1 EGTA, 14 Creatine phosphate, 4 MgATP, 0.3 GTP (Tris salt) and 10 HEPES (pH 7.2, CsOH). In experiments targeting hNa$_V$1.8 in ND7/23 cells or TTX-R currents in TG neurons, 100 nM TTX was added to all external and working solutions to eliminate TTX-sensitive (TTX-S) sodium currents. In TG neurons, sodium currents were evoked by depolarizing steps from a holding potential of −80 mV to test potentials ranging from −80 mV to +10 mV in 10 mV increments. For hNa$_V$1.7 and hNa$_V$1.8 recordings, currents were evoked by depolarizing steps from a holding potential of −80 mV to test potentials ranging from −80 mV to +30 mV in 10 mV increments. Step durations were 100 ms for TTX-S and TTX-R current recordings.

To assess the voltage dependence of TTX-R sodium current activation in TG neurons, 100 ms depolarizing steps were applied from a holding potential of −80 mV to test potentials ranging from −80 mV to +30 mV in 10 mV increments. The voltage of half-maximal activation ($V_{0.5}$) was estimated by calculating the macroscopic conductance (G) at each test potential using the extended Ohm's law: $G = I_{peak}/(V_{test} - V_{rev})$, where I_{peak} is the peak current amplitude, V_{test} is the test potential, and V_{rev} is the apparent sodium reversal potential, determined individually for each cell. Conductance-voltage (G-V) relationships were then fitted with a Boltzmann function: $G = G_{max}/(1 + \exp[(V_{0.5} - V_M)/k])$, where G_{max} is the maximal conductance, V_M is the membrane potential, $V_{0.5}$ is the voltage at which half of the channels are activated, and k is the slope factor (in mV).

Availability curves of TTX-R sodium currents were obtained using a double-pulse protocol. A 120 ms conditioning prepulse was applied from a holding potential of −80 mV to voltages ranging from −120 mV to +20 mV in 10 mV increments, followed by a 20 ms test pulse to 0 mV. The peak current during the test pulse was normalized to the maximal response and plotted as mean ± SEM versus the prepulse voltage. The resulting data were fitted with a Boltzmann equation: $I_{test}/I_{max} = 1/(1+ \exp[(V - V_{0.5})/k])$, where V is the conditioning pulse voltage, $V_{0.5}$ is the voltage at which half the channels are available, and k is the slope factor (in mV).

To evaluate the voltage dependence of activation for Na$_V$ isoforms, 100 ms depolarizing steps were applied from a holding potential of −80 mV to test potentials ranging from −80 mV to +20 mV in 10 mV increments. For Na$_V$1.8, the test range was extended up to +50 mV. The voltage of half-maximal activation ($V_{0.5}$) was determined as explained above.

Availability curves for all Na$_V$ isoforms were obtained using a double-pulse protocol. A 50 ms conditioning pulse from a holding potential of −80 mV was applied to voltages ranging from −120 mV to +20 mV in 10 mV increments, followed by a 30 ms test pulse to −10 mV. For Na$_V$1.8, the test pulse was to +10 mV and extended to 100 ms. The peak current during the test pulse was normalized to the maximal current and plotted as mean ± SEM against the conditioning voltage. Data were fitted with a Boltzmann function as explained above.

A state-dependent block of hNa$_V$1.8 current was established using the following protocol [20]: 10 s long conditioning pulses (V_{cond}) were applied from a holding potential of −120 mV. The amplitude of the conditioning pulses varied systematically (in 10 mV steps) between -120 and 0 mV. Then, a 100 ms step to −120 mV was applied to remove fast inactivation, followed by a 5 ms test pulse (V_{test}) to +10 mV. The resulting hNa$_V$1.8 current amplitude was normalized to the maximal current amplitude (fraction available) and plotted (mean ± SEM) versus the voltage of conditioning pulses. The data were fitted using the Boltzmann equation, $I_{test}/I_{max} = 1/(1+ \exp[(V - V_{0.5})/k])$, where V is the conditioning pulse potential, $V_{0.5}$ is the potential at which one-half of the channels are available. k is the slope factor (in mV).

A state-dependent block of hNa$_V$1.7 current was assessed using the following protocol [8]: 5 s long conditioning pulses (V_{cond}) were applied from a holding potential of −80 mV. The amplitude of the conditioning pulses varied systematically (in 10 mV steps) between −120 and −20 mV and was followed by a 10 ms test pulse (V_{test}) to −10 mV. The resulting hNa$_V$1.7 current amplitude was normalized to the maximal current amplitude (fraction available) and plotted (mean ± SEM) versus the voltage

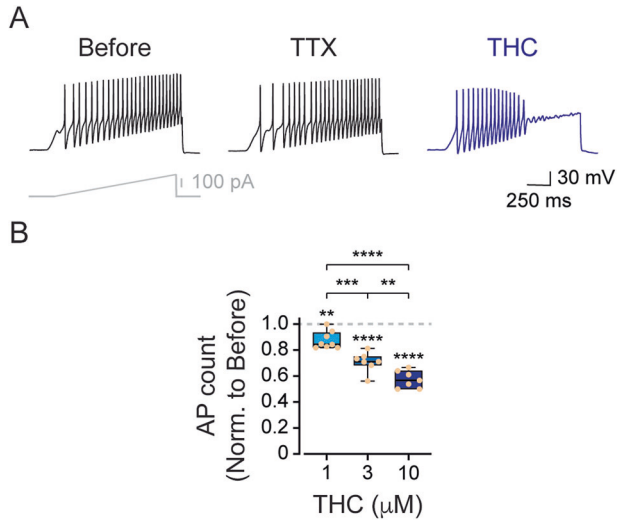

Fig. 1 THC inhibits nociceptive firing. A Representative whole-cell current-clamp recording from acutely dissociated rat nociceptive TG neurons in response to a current ramp (300 pA in 1 s; *inset*) before (*left*), during exposure to 0.1 μM TTX (*middle*), and during exposure to 10 μM THC (*right*). **B** Concentration-response relationship for inhibition of the AP firing by THC in nociceptor TG neurons. Box plots and individual values demonstrate changes in the number of APs following 4 min of exposure to THC at the indicated concentrations. The number of action potentials was normalized to the number of evoked action potentials before the application of THC. One-way ANOVA, followed by Bonferroni's post hoc test when **, $p \le 0.01$; ***, $p \le 0.001$; ****, $p \le 0.0001$.

of conditioning pulses. The data were fitted using Boltzmann equation $I_{test}/I_{max} = 1/(1+ \exp[(V - V_{1/2})/k])$, where V is the conditioning pulse potential, $V_{1/2}$ is the potential at which one-half of the channels are available, and k is the slope factor (in mV).

To evaluate the effects of THC on T-type calcium currents, the following solutions were used [21]: The extracellular solution contained (in mM): 10 $BaCl_2$, 152 tetraethylammonium chloride (TEA-Cl), and 10 HEPES, with the pH adjusted to 7.4 using TEAOH. The intracellular solution contained (in mM): 135 tetramethylammonium hydroxide, 10 EGTA, 40 HEPES, and 2 $MgCl_2$, with the pH adjusted to 7.2 using hydrofluoric acid.

T-type calcium currents were recorded by holding the membrane potential at −90 mV and applying depolarizing voltage steps from −80 mV to +60 mV in 10 mV increments, each lasting 250 ms. Current amplitude was determined by measuring the peak inward current and subtracting the current remaining at the end of the depolarizing pulse to minimize contamination from residual high-voltage–activated currents.

Statistical analysis

The electrophysiological analysis was performed offline using Clampfit 10.7 software (Molecular Devices, USA). Fitting and statistical analysis were done using Prism 10 software (Graphpad Software Inc., USA). Data were compared by one or two-way analysis of variance (ANOVA) with the Bonferroni post hoc test and considered statistically significant when $p \le 0.05$. The box plots depict the mean and the 25th–75th percentiles, with whiskers indicating the minimum and maximum values. Otherwise, the data are presented as the mean ± SEM.

The count of action potentials in current-clamp recordings was established by detecting instances when the voltage crossed a specific threshold above the resting potential. Only neurons that demonstrated a stable resting potential and stable action potential threshold with no significant change in the action potential frequency-intensity relationship during the application of the extracellular solution were analyzed.

In voltage-clamped cells, concentration-response curves were calculated as the peak current amplitude evoked by depolarizing steps normalized to the control peak amplitude measured without drugs. Leak subtraction was applied before the normalization of the current amplitude. The peak currents were averaged and fitted to a non-linear sigmoidal concentration-response (variable slope) equation in GraphPad Prism software. Cells exhibiting drift or inconsistent baseline current were excluded from the analysis.

RESULTS

THC suppresses action potential firing in nociceptor neurons

To evaluate the direct effect of THC on nociceptor excitability, we performed whole-cell current-clamp recordings from acutely dissociated rat nociceptor (≤ 25 μm) trigeminal ganglion (TG) neurons. Neurons were stimulated with a ramp current protocol (300 pA over 1 s), reliably evoking repetitive action potentials under control conditions (Fig. 1A, left). As expected, the application of tetrodotoxin (TTX, 100 nM) slightly reduced firing, suggesting the expression of TTX-resistant sodium channels, a key feature of nociceptors [22–24] (Fig. 1A, middle). Notably, application of THC (10 μM) resulted in a robust suppression of action potential firing (Fig. 1A, right and Fig. S1A). This THC-induced inhibition of nociceptors' firing was also significant at lower concentrations (i.e., 1 and 3 μM) (Fig. 1B). For experimental validation, we also analyzed the effect of CBD on nociceptors' firing, and as previously reported [7, 25], CBD induced a pronounced inhibition of firing (Fig. S1B, C). These results demonstrate that THC directly reduces the excitability of nociceptive neurons.

In nociceptor neurons, THC preferentially inhibits TTX-R sodium currents

Because THC inhibits action potential firing despite the presence of TTX, it suggests that THC acts on TTX-resistant (TTX-R) sodium channels. TTX-R sodium currents provide the main inward current component of the action potentials and underlie the ability of nociceptors to fire repeatedly [22, 23, 26, 27]. Therefore, we first examine the effect of THC on the amplitude of TTX-R sodium current in nociceptor TG neurons. THC (10 μM) significantly reduced the peak TTX-R sodium current by ~35% (Fig. 2A). Application of THC led to a significant and prominent (~11 mV, $p = 0.007$, paired t-test, $n = 8$ neurons) rightward shift in the voltage dependence of activation of TTX-R currents (Fig. 2B). Moreover, it produced a significant leftward shift in the voltage dependence of fast inactivation of ~ 6 mV ($p = 0.0004$, paired t-test, $n = 7$ neurons, Fig. 2C). Notably, the application of THC substantially enhanced the slow inactivation of TTX-R current by significantly shifting its voltage dependence to the left by ~11 mV ($p = 0.0002$, paired t-test, $n = 6$ neurons) (Fig. 2D).

We next examined the effect of THC sodium current on large (≥35 μm) non-nociceptive TG neurons. These neurons express mainly TTX-S sodium channels [28, 29]. THC (10 μM) slightly but significantly reduced the peak of TTX-S sodium current by ~15% (Fig. S2A, B). Notably, the effect of THC on these currents was significantly smaller than on TTX-R currents in nociceptor neurons (Fig. S2C). Altogether, our results demonstrate that THC inhibits both TTX-R and TTX-S currents, but to a different extent. The higher efficacy of THC for TTX-R current implies a preferential effect of THC on nociceptor neurons.

THC selectively inhibits $Na_V1.7$ and $Na_V1.8$ nociceptive sodium channels

Nociceptive neurons express both TTX-R $Na_V1.8$ and TTX-S $Na_V1.7$ isoforms [11]. Therefore, we examined the effect of THC on human $Na_V1.8$ ($hNa_V1.8$) and human $Na_V1.7$ ($hNa_V1.7$) expressed in heterologous systems. To express $hNa_V1.8$, we used ND7/23 cells that enable the expression of this channel [30], and $hNa_V1.7$ was expressed in HEK293T cells. The application of THC (10 μM) substantially reduced both $hNa_V1.8$ and $hNa_V1.7$ induced currents (Fig. 3A). The effect of THC on both channels was concentration-dependent, with similar potency and efficiency (Fig. 3B). These results demonstrate that THC is an inhibitor of $Na_V1.7$ and $Na_V1.8$ nociceptive sodium channels.

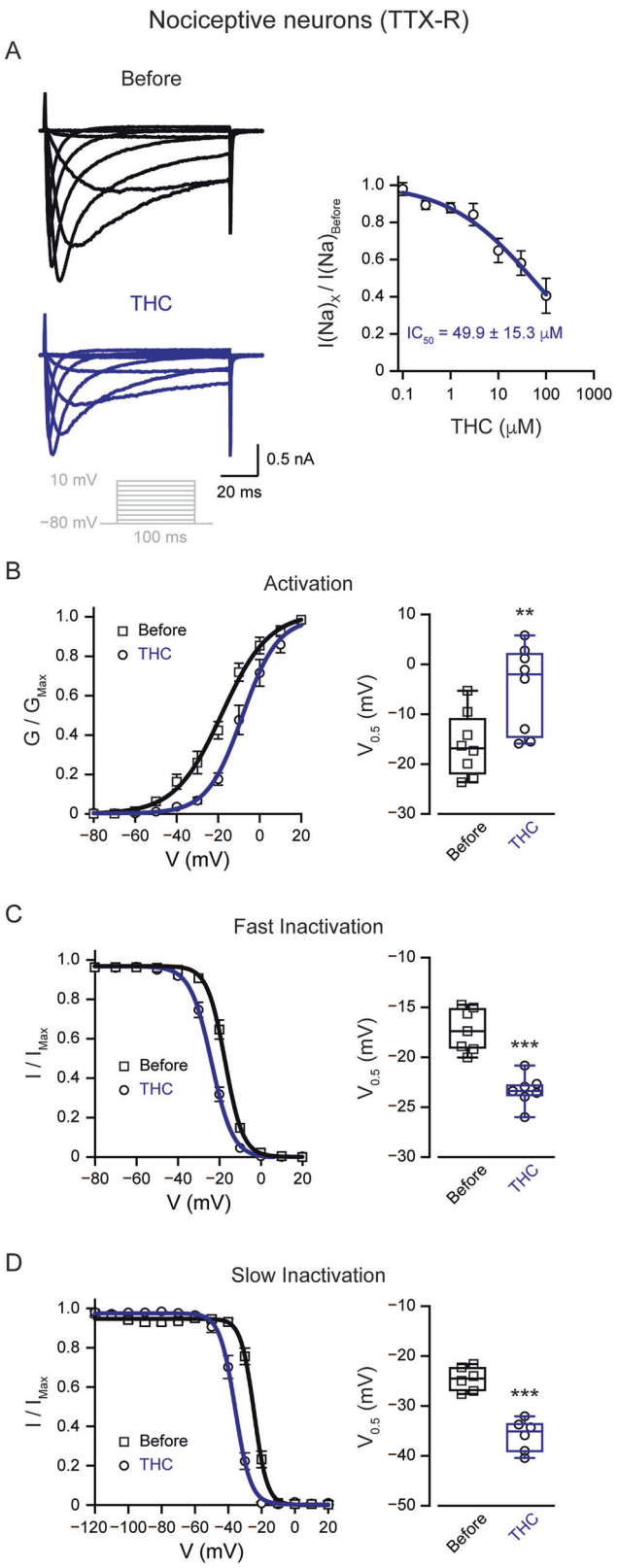

Fig. 2 THC inhibits nociceptive sodium currents. A *Right:* Representative whole-cell voltage-clamp recording of TTX-R sodium currents from acutely dissociated rat nociceptive TG neurons before (*upper*) and after exposure to THC (10 μM; *lower*). Currents were elicited by depolarizing steps from a holding potential of −80 mV to 10 mV in 10 mV increments (*inset*). *Left:* Concentration-response relationship of TTX-R sodium currents amplitude (normalized to the current before the application of THC) following 4 min of exposure to THC at the indicated concentrations. The solid line represents the fit of the Hill equation. **B–C** *Left:* G/G_{max} (activation; (**B**) and I/I_{max} (availability; (**C**) curves for TTX-R sodium current before (*squares*) and 4 min after the application of 10 μM THC (*circles*). Note that THC induced a rightward shift in activation and a leftward shift in inactivation. To assess the voltage dependence of activation, 100-ms depolarizing steps were applied to a range of test potentials in 10 mV increments, from a holding potential of −80 mV to +30 mV. For the voltage dependence of fast inactivation, a double pulse protocol was used: a prepulse (V_{cond}) was held constant at 120 ms and its amplitude was varied between −120 and +20 mV. I_{test} was assessed by stepping to 0 mV for 20 ms. The membrane was held at −80 mV. *Right:* Box plot and individual paired values of $V_{0.5}$ of activation (**B**) and inactivation (**C**). Paired Student's *t* test when **, $p \le 0.01$; ***, $p \le 0.001$. **D** *Left:* Voltage-dependence of TTX-R sodium currents steady-state channel availability (Fraction available, I/I_{max}, plotted as a function of conditioning pulse voltage) before (*squares*) and 4 min (*circles*) after the application of 10 μM THC. V_{cond} was held constant at 10 s, and its amplitude was varied between −120 and 0 mV. 100 ms step to −120 mV was applied before V_{test}. I_{test} was evoked by stepping to +10 mV for 5 ms. The membrane was held at −120 mV. Solid lines: fits to the Boltzmann function. Note a substantial decrease in channel availability following the treatment with THC. *Right:* Box plot and individual paired values of $V_{0.5}$ of voltage-dependence of steady-state channel availability before and 4 min after the application of 10 μM THC. Paired Student's *t* test when ***, $p \le 0.001$.

To further examine the specificity of THC to $Na_V1.7$ and $Na_V1.8$ channels, we analyzed its effect on all non-nociceptive specific sodium channels isoforms ($hNa_V1.1$-1.6). In contrast to the non-psychoactive cannabinoid CBD [6], THC did not affect the amplitude of $hNa_V1.1$-1.6 currents (Fig. 3C). Notably, THC demonstrates a significant inhibition of $hNa_V1.7$-1.8 in comparison to other isoforms (Fig. 3C). No difference in THC effect between $hNa_V1.7$ and $hNa_V1.8$ was observed.

THC inhibits $Na_V1.7$ and $Na_V1.8$ nociceptive sodium channels via the local anesthetic binding site

It has been shown that non-psychoactive cannabinoids inhibit sodium channels by stabilizing the inactivated state [6, 8, 10]. To examine whether THC acts via similar mechanisms, we tested whether THC induces a state-dependent block of $Na_V1.7$ and $Na_V1.8$ channels. We found that THC induces a significant left-ward shift of ~13 mV in the $V_{1/2}$ of $hNa_V1.8$ and a left-ward shift of ~6 mV in the $V_{1/2}$ of $hNa_V1.7$ (Fig. 4A, B). These results show that THC-induced inhibition of sodium channels is state-dependent, resembling local-anesthetic (LA) induced inhibition. Hence, we hypothesize that THC acts similarly to local anesthetics.

To examine this hypothesis, we tested whether classical mutations in this binding site of $hNa_V1.8$ affect the THC inhibition [14]. We found that even a single F1759A mutation was sufficient to reduce the THC potency by about half a log (Fig. 4C). Adding the Y1766A mutation resulted in further reduction of THC potency to the level that the exact efficacy cannot be directly assessed (Fig. 4C). Moreover, the double LA binding site mutation abolished THC-induced state-dependent block (Fig. 4D). These data strongly suggest that THC acts through the LA binding site.

$hNa_V1.8$, but not $hNa_V1.7$, has different susceptibility to phytocannabinoids

We next compared the effects of THC on $hNa_V1.7$ and $hNa_V1.8$ channels with those of the non-psychoactive phytocannabinoids cannabidiol (CBD), cannabigerol (CBG), and cannabichromene (CBC).

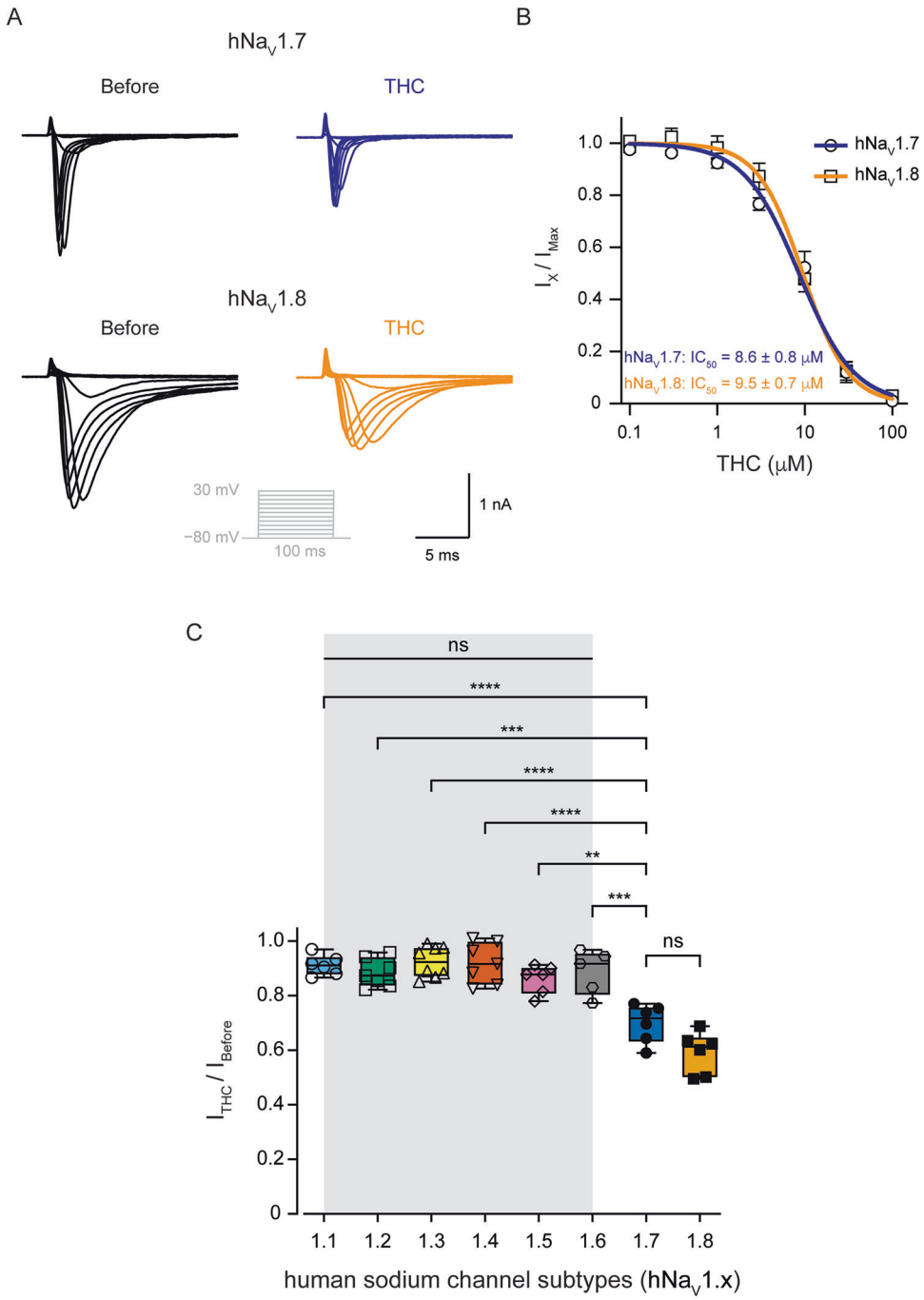

Fig. 3 THC selectively inhibits the nociceptive hNa$_V$1.8 and hNa$_V$1.7 channels. A Representative whole-cell voltage-clamp recording from hNa$_V$1.7 expressed in HEK293T cells (*upper*) and hNa$_V$1.8 expressed in ND7/23 cells (*lower*) before (*left*) and after exposure to THC (10 μM; *right*). Currents were elicited by depolarizing steps from a holding potential of −80 mV to 30 mV in 10 mV increments (*inset*). **B** Concentration-response relationship for inhibition of hNa$_V$1.7 (*circles*) and hNa$_V$1.8 (*squares*) channels by THC. Each dot represents the mean and SEM of at least $n = 6$ cells. IC_{50} were determined by fitting Hill's function to the data (shown as *blue and orange curves* for hNa$_V$1.7 and hNa$_V$1.8, respectively). **C** Box plots and individual values summarizing the inhibitory effect of 10 μM THC on the peak current of hNa$_V$ channels. The current values are normalized to the value before the application of THC. Note that THC does not affect non-nociceptive specific sodium channel isoforms. One-way ANOVA, followed by Bonferroni's post hoc test when ns not significant; **, $p \leq 0.01$; ***, $p \leq 0.001$; ****, $p \leq 0.0001$.

We found that the effect of THC on hNa$_V$1.7 was similar to that of non-psychoactive cannabinoids (Fig. 5A). However, the effect of THC on hNa$_V$1.8 was similar to that of CBC but substantially weaker than the effect of CBD and CBG (Fig. 5B). Hence, our results suggest that while hNa$_V$1.7 is affected similarly by all examined phytocannabinoids, hNa$_V$1.8 discriminates between them.

DISCUSSION

The analgesic properties of cannabis are often attributed to the central actions of Δ^9-tetrahydrocannabinol (THC), mediated by cannabinoid receptors [3, 31]. Here, we identify a distinct, non-canonical peripheral mechanism of action for THC, which may contribute to its analgesic efficacy. Our findings suggest that THC directly inhibits peripheral nociceptor excitability through the

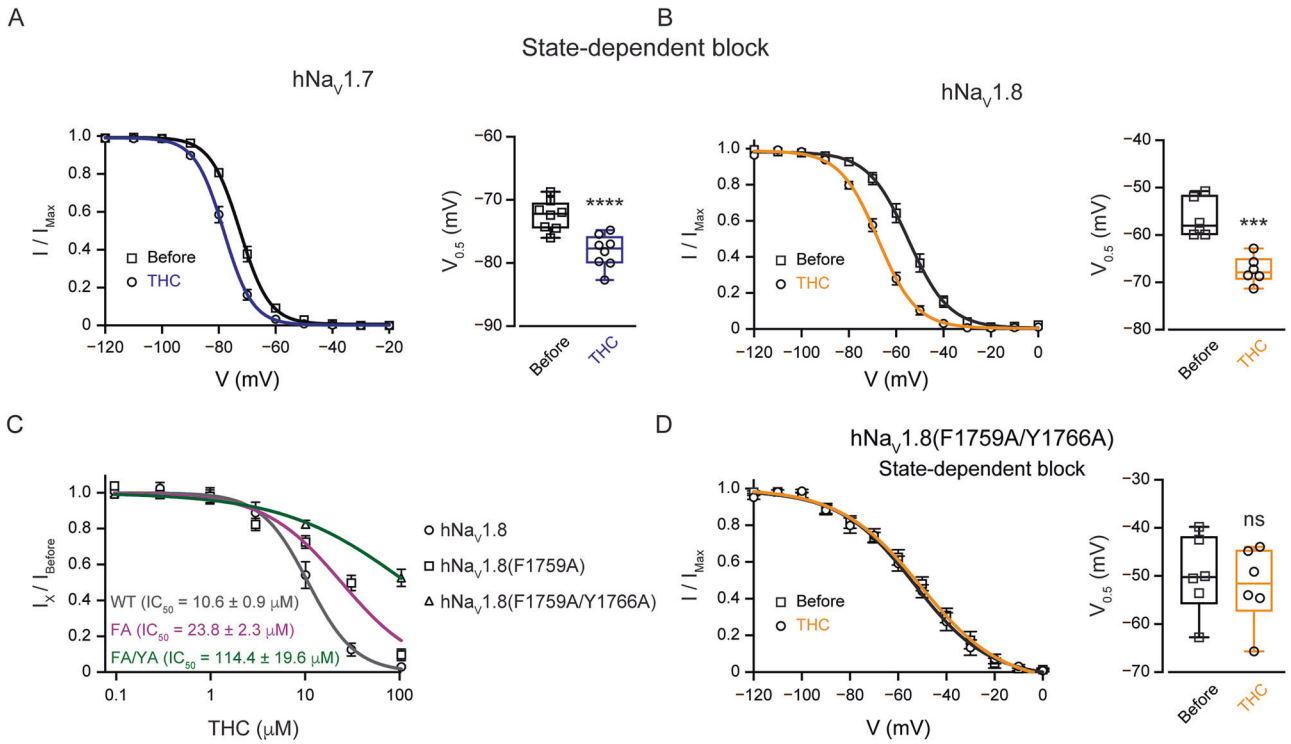

Fig. 4 THC inhibits $hNa_V1.7$ and $hNa_V1.8$ channels via the local anesthetic binding site. A *Left:* Voltage-dependence of $hNa_V1.7$ steady-state channel availability (I/I_{max}), plotted as a function of conditioning pulse voltage before (squares) and after the application of THC (circles). Solid lines represent fits to a Boltzmann function. *Right:* Box plot and individual values of the half-inactivation potential ($V_{0.5}$) before and after THC treatment. **B** Same as (**A**), but recorded from cells expressing $hNa_V1.8$ channels before (squares) and after the application of THC (circles). Note the significant hyperpolarizing shift in the voltage dependence of inactivation for both channels, indicating that THC stabilizes the inactivated state. Paired Student's *t* test when ***, $p \leq 0.001$; ****, $p \leq 0.0001$. **C** Concentration-response relationship for the inhibition of wild-type (WT) and mutated $hNa_V1.8$ channels by THC. Data points represent the current inhibition for WT (circles; black line), the F1759A mutant (FA; squares; pink line), and the F1759A/Y1766A double mutant (FA/YA; triangles; green line) at various THC concentrations. The indicated IC_{50} values were determined by fitting Hill's function to the data. Note the substantial rightward shift of the curves for the mutated channels, indicating a significant reduction in inhibitory potency. **D** Voltage-dependence of mutated $hNa_V1.8$ (F1759A/Y1766A) steady-state channel availability (I/I_{max}), plotted as a function of conditioning pulse voltage before (squares) and after the application of THC (circles). Solid lines represent fits to a Boltzmann function. *Right:* Box plot and individual values of the half-inactivation potential ($V_{0.5}$) before and after THC treatment. Note that in the mutated $hNa_V1.8$, THC does not lead to a change in the state-dependent block.

modulation of voltage-gated sodium channels $hNa_V1.7$ and $hNa_V1.8$. This suppression is facilitated by a direct, state-dependent interaction with the conserved local anesthetic (LA) binding site, establishing a peripheral analgesic pathway for THC that operates independently of cannabinoid receptor signaling.

The physiological significance of this mechanism is demonstrated by the suppression of action potential firing in nociceptive trigeminal ganglion neurons upon THC application. While our data suggest that THC's efficacy in reducing action potential firing is lower than that reported for non-psychoactive cannabinoids such as CBD and CBG, its effect is nonetheless robust [6, 7, 9, 10] (Fig.S1). Moreover, we demonstrate that THC inhibits both TTX-S and TTX-R sodium currents. The smaller, yet significant, reduction of the TTX-S current in native nociceptors aligns with our finding that THC potently inhibits $Na_V1.7$ while exerting no effect on other TTX-S isoforms ($Na_V1.1$-1.6), thereby identifying $Na_V1.7$ as the primary TTX-S target in these neurons.

Our investigation into specific sodium channel isoforms offers further clarification of this mechanism. The high selectivity that THC exhibits for the nociceptive channels $hNa_V1.7$ and $hNa_V1.8$ over other sodium channel isoforms is striking. However, previous studies have shown that $Na_V1.7$ expression is broadly expressed across sensory neuron populations, including non-nociceptive neurons, with the highest levels in C-low-threshold mechanoreceptors [32]. In contrast, $Na_V1.8$ exhibits more restricted expression, being predominantly found in nociceptors but also present in select mechanoreceptor populations [33]. Nevertheless, recent evidence from human DRG neurons [34] underscores the importance of the complementary interplay between $Na_V1.7$ and $Na_V1.8$ in defining nociceptor firing. $Na_V1.7$ primarily governs the threshold and initial upstroke of the action potential, whereas $Na_V1.8$ activates more gradually, considerably contributing to the peak amplitude and the characteristic shoulder of the action potential, and playing a critical role in maintaining repetitive firing [12, 26, 35, 36]. The dual inhibition of $Na_V1.7$ and $Na_V1.8$ by THC may provide greater therapeutic selectivity for nociceptors by leveraging their complementary roles in pain signal generation and transmission.

Our data demonstrate that THC affects neuronal and heterologously expressed sodium channels differently (compare Figs. 2A and 3B). This apparent mismatch could stem from the difference between the two experimental systems. The dose-response curve in Fig. 2A was generated from native neuronal preparations that contain a heterogeneous population of voltage-gated sodium channel subtypes. As we show in Fig. 3C, these subtypes have distinct sensitivities to THC. The resulting curve therefore represents the composite response of the entire population, plausibly obscuring the higher affinity of the most sensitive channel isoforms. In contrast, the experiment in Fig. 3B is performed on a homogeneous channel population ($Na_V1.7$ or $Na_V1.8$), revealing almost complete inhibition at 30 μM. Additionally, species-specific differences between the rodent channels in

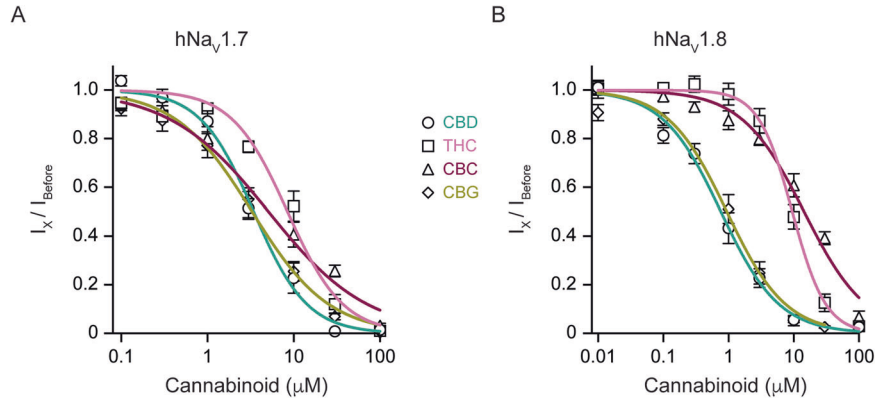

Fig. 5 hNa$_V$1.7 and hNa$_V$1.8 channels exhibit differential sensitivity to phytocannabinoids. A Concentration-response curves for the inhibition of hNa$_V$1.7 channels by cannabidiol (CBD; circles), Δ⁹-tetrahydrocannabinol (THC; squares), cannabichromene (CBC; triangles), and cannabigerol (CBG; diamonds). Peak current amplitude was normalized to the current before drug application (I_X/I_{Before}) and plotted against the cannabinoid concentration. Solid lines represent fits of the data to the Hill equation. Each data point represents the mean ± SEM from at least $n = 6$ cells. hNa$_V$1.7: [CBD: $IC_{50} = 3.4 \pm 0.3$ μM; THC: $IC_{50} = 8.4 \pm 0.8$ μM; CBC: $IC_{50} = 5.1 \pm 0.7$ μM; CBG: $IC_{50} = 3.3 \pm 0.3$ μM]. **B** Same as (**A**), but for hNa$_V$1.8 channels. hNa$_V$1.8: [CBD: $IC_{50} = 0.8 \pm 0.1$ μM; THC: $IC_{50} = 9.5 \pm 0.6$ μM; CBC: $IC_{50} = 14.4 \pm 1.4$ μM; CBG: $IC_{50} = 0.9 \pm 0.1$ μM].

our native preparation and the human channels used for heterologous expression could contribute to the observed shift in potency.

Is the THC-induced inhibition of Na$_V$1.7 and Na$_V$1.8 the sole mechanism underlying its effect on nociceptor excitability? It has been shown that THC also inhibits T-type voltage-gated calcium channels (VGCC) [37, 38]. We also found that THC inhibits T-type VGCC in nociceptors, albeit with lesser potency than TTX-R channels (Fig. S3). These results imply that THC-induced inhibition of nociceptor excitability could result from its combined effect on Na$_V$s and T-type calcium channels. Moreover, previous studies have demonstrated that primary nociceptor neurons express CB1R [39, 40]. Furthermore, we and others showed that THC directly activates TRPA1 channels that are also expressed in a subpopulation of nociceptors [41–44]. Consequently, THC may modulate neuronal excitability also via its effects on CB1R or TRPA1. However, whether these interactions will increase or decrease neuronal excitability (due to desensitization or depolarizing block) remains to be determined.

The leftward shift in the voltage dependence of both fast and slow inactivation induced by THC is characteristic of state-dependent channel blockers that preferentially stabilize inactivated states [45, 46]. This profile is consistent with the action of local anesthetics [47, 48]. Indeed, mutagenesis of key residues within the LA binding site of hNa$_V$1.8 (F1759A and Y1766A) significantly attenuated the inhibitory effect of THC and abrogated its state-dependent properties. These data provide strong evidence that THC interacts directly with this conserved site, aligning the mechanism of a major phytocannabinoid with a classical pathway for local anesthesia.

Notably, the dose-response curve of THC's effect on nociceptors' TTX-R sodium currents is relatively shallow with a negative Hill slope of 0.50 ± 0.09 (Fig. 2A). Such a slope could result from THC's effects on the heterogeneous population of neuronal channels. On the other hand, the apparent shallowness may not reflect the actual dose-response relation of THC, but a technical limitation of THC solubility rather than a pure biological effect. THC is highly hydrophobic (log P~7) with minimal aqueous solubility (~0.26 μg/mL) [49–52]. Hence, at high concentrations, THC precipitates out of solution via salt-out effects, preventing us from achieving a true pharmacological plateau. Consequently, our dose-response curve only partially captures the inhibition profile, resulting in an apparent Hill slope <1. This incomplete curve shape is well documented in studies of lipophilic drugs [53].

We found that the effects of THC on neuronal sodium currents occur at IC_{50} values in the high micromolar range (Fig. 2A). Are these doses physiologically relevant? Our results demonstrate a significant effect on neuronal firing already with 1 μM THC (Fig. 1). The IC_{50} values for the human sodium channels Na$_V$1.7 and Na$_V$1.8 are approximately 10 μM (Fig. 3). These nominal concentrations are indeed higher than the expected concentration of THC following cannabis consumption, which ranges between 0.1 and 1 μM within 3–10 min, coinciding with the onset of analgesia as reported in clinical trials [54–56]. However, the nominal aqueous concentrations used in our electrophysiological recordings do not directly reflect the effective concentrations at the lipid membrane-channel interface for a compound as lipophilic as THC. As previously demonstrated, THC partitions rapidly into cellular membranes, reaching local microenvironments in which its activity is substantially higher than that suggested by bulk solution levels [49, 57, 58]. Indeed, human pharmacokinetic and tissue-distribution studies demonstrate that after inhalation or vaporization, rapid redistribution of THC to lipid-rich tissues such as fat, skin, muscle, or nerve yields tissue/plasma ratios of 10–50, with measured local THC concentrations of 5–30 μM [56, 59–62]. These levels are well within the range required to produce Na$_V$1.7/1.8 inhibition, as we showed in Fig. 3. Therefore, the direct modulation of peripheral nociceptor sodium channels can contribute to analgesia following THC consumption.

A comparison of THC with other phytocannabinoids under identical experimental conditions reveals significant pharmacological distinctions. Our findings demonstrate that, while hNa$_V$1.7 is a relatively promiscuous target, being inhibited with comparable potency by THC, CBD, CBG, and CBC, hNa$_V$1.8 functions as a molecular discriminator. This channel exhibited markedly lower sensitivity to THC and CBC in comparison to CBD and CBG. Such isoform-specific selectivity indicates that, despite sharing a common binding site, subtle structural variations among phytocannabinoids are sufficient to modify binding affinity within the hNa$_V$1.8 channel. Specifically, THC and CBC both contain cyclic ether rings, whereas CBD features an open pyran ring, and CBG is an acyclic precursor [63]. It is well recognized that the rigid, closed pyran ring of THC is crucial for its high-affinity binding to the CB1 receptor and the subsequent psychoactive effects [31]. Consequently, it is plausible that these cyclic structures in THC and CBC may be less optimal for interaction with the LA binding site of Na$_V$1.8 compared to the more flexible conformations of CBD and CBG. This observation enhances the understanding of the molecular pharmacology of the LA binding site and suggests potential directions for future structure-activity relationship studies aimed at designing cannabinoid derivatives with specific isoform selectivity.

In summary, this study provides evidence for an additional aspect of THC's pharmacology. Besides its central receptor-mediated effects, THC also acts as a direct peripheral inhibitor of nociceptive sodium channels $hNa_V1.7$ and $hNa_V1.8$ through the local anesthetic binding site. Although it may be less potent than other phytocannabinoids in reducing overall firing, its high selectivity for $Na_V1.7$ and $Na_V1.8$ nociceptive sodium channels makes it an effective modulator of peripheral pain signaling. These findings help to clarify the peripheral analgesic effects of cannabis. Additionally, it suggests that developing peripherally restricted THC analogs could offer pain relief with fewer central nervous system side effects, opening a new potential direction for pain management strategies.

DATA AVAILABILITY

All data needed to evaluate the conclusions are presented in the paper. All the data and materials are fully available upon request from the corresponding authors.

REFERENCES

1. Vučkovic S, Srebro D, Vujovic KS, Vučetic Č, Prostran M. Cannabinoids and pain: new insights from old molecules. Front Pharmacol. 2018;9:1–19.
2. Hill KP, Palastro MD, Johnson B, Ditre JW. Cannabis and pain: a clinical review. Cannabis Cannabinoid Res. 2017;2:96–104.
3. Pertwee RG. The pharmacology of cannabinoid receptors and their ligands: an overview. Int J Obes. 2006;30:13–18.
4. Huestis MA, Gorelick DA, Heishman SJ, Preston KL, Nelson RA, Moolchan ET, et al. Blockade of effects of smoked marijuana by the CB1-selective cannabinoid receptor antagonist SR141716. Arch Gen Psychiatry. 2001;58:322–8.
5. Stella N. THC and CBD: similarities and differences between siblings. Neuron. 2023;111:302–27.
6. Ghovanloo MR, Shuart NG, Mezeyova J, Dean RA, Ruben PC, Goodchild SJ. Inhibitory effects of cannabidiol on voltage-dependent sodium currents. J Biol Chem. 2019;293:16546–58.
7. Zhang HXB, Bean BP. Cannabidiol inhibition of murine primary nociceptors: tight binding to slow inactivated states of Nav1.8 channels. J Neurosci. 2021;41:6371–87.
8. Huang J, Fan X, Jin X, Jo S, Zhang HB, Fujita A, et al. Cannabidiol inhibits Na(v) channels through two distinct binding sites. Nat Commun. 2023;14:3613.
9. Ghovanloo M-R, Tyagi S, Zhao P, Waxman SG. Nav1.8, an analgesic target for nonpsychotomimetic phytocannabinoids. Proc Natl Acad Sci USA. 2025;122:e2416886122.
10. Ghovanloo M-R, Estacion M, Higerd-Rusli GP, Zhao P, Dib-Hajj S, Waxman SG. Inhibition of sodium conductance by cannabigerol contributes to a reduction of dorsal root ganglion neuron excitability. Br J Pharmacol. 2022;179:4010–30.
11. Hameed S. Nav1.7 and Nav1.8: role in the pathophysiology of pain. Mol Pain. 2019;15:1744806919858801.
12. Dib-Hajj SD, Cummins TR, Black JA, Waxman SG. Sodium channels in normal and pathological pain. Annu Rev Neurosci. 2010;33:325–47.
13. Bhattacharya A, Wickenden AD, Chaplan SR. Sodium channel blockers for the treatment of neuropathic pain. Neurotherapeutics. 2009;6:663–78.
14. Ragsdale DS, McPhee JC, Scheuer T, Catterall WA. Molecular determinants of state-dependent block of Na+ channels by local anesthetics. Science. 1994;265:1724–8.
15. Maatuf Y, Kushnir Y, Nemirovski A, Ghantous M, Iskimov A, Binshtok AM, et al. The analgesic paracetamol metabolite AM404 acts peripherally to directly inhibit sodium channels. Proc Natl Acad Sci USA. 2025;122:e2413811122.
16. Pertwee RG, Howlett AC, Abood ME, Alexander SPH, Di Marzo V, Elphick MR, et al. International Union of Basic and Clinical Pharmacology. LXXIX. Cannabinoid receptors and their ligands: beyond CB_1 and CB_2. Pharmacol Rev. 2010;62:588–631.
17. Hazan A, Kumar R, Matzner H, Priel A. The pain receptor TRPV1 displays agonist-dependent activation stoichiometry. Sci Rep. 2015;5:1–13.
18. Geron M, Kumar R, Matzner H, Lahiani A, Gincberg G, Cohen G, et al. Protein toxins of the Echis coloratus viper venom directly activate TRPV1. Biochim Biophys Acta Gen Subj. 2017;1861:615–23.
19. Kumar R, Hazan A, Basu A, Zalcman N, Matzner H, Priel A. Tyrosine residue in the TRPV1 vanilloid binding pocket regulates deactivation kinetics. J Biol Chem. 2016;291:13855–63.
20. Leffler A, Reiprich A, Mohapatra DP, Nau C. Use-dependent block by lidocaine but not amitriptyline is more pronounced in tetrodotoxin (TTX)-Resistant Nav1.8 than in TTX-sensitive Na+ channels. J Pharmacol Exp Ther. 2007;320:354–64.
21. Jagodic MM, Pathirathna S, Nelson MT, Mancuso S, Joksovic PM, Rosenberg ER, et al. Cell-specific alterations of T-type calcium current in painful diabetic neuropathy enhance excitability of sensory neurons. J Neurosci J Soc Neurosci. 2007;27:3305–16.
22. Blair NT, Bean BP. Roles of tetrodotoxin (TTX)-sensitive Na+ current, TTX-resistant Na+ current, and Ca2+ current in the action potentials of nociceptive sensory neurons. J Neurosci. 2002;22:10277–90.
23. Renganathan M, Cummins TR, Waxman SG. Contribution of Nav1. 8 sodium channels to action potential electrogenesis in DRG neurons. J Neurophysiol. 2001;86:629–40.
24. Bennett DL, Clark XAJ, Huang J, Waxman SG, Dib-Hajj SD. The role of voltage-gated sodium channels in pain signaling. Physiol Rev. 2019;99:1079–151.
25. Chahyadinata G, Nam JH, Battenberg A, Wainger BJ. Physiological profiling of cannabidiol reveals profound inhibition of sensory neurons. Pain. 2024;165:2544–53.
26. Gudes S, Barkai O, Caspi Y, Katz B, Lev S, Binshtok AM. The role of slow and persistent TTX-resistant sodium currents in acute tumor necrosis factor-α-mediated increase in nociceptor excitability. J Neurophysiol. 2015;113:601–19.
27. Tan Z-Y, Piekarz AD, Priest BT, Knopp KL, Krajewski JL, McDermott JS, et al. Tetrodotoxin-resistant sodium channels in sensory neurons generate slow resurgent currents that are enhanced by inflammatory mediators. J Neurosci J Soc Neurosci. 2014;34:7190–7.
28. Chahine M, O'Leary ME. Regulation/modulation of sensory neuron sodium channels. Handb Exp Pharmacol. 2014;221:111–35.
29. Caffrey JM, Eng DL, Black JA, Waxman SG, Kocsis JD. Three types of sodium channels in adult rat dorsal root ganglion neurons. Brain Res. 1992;592:283–97.
30. John VH, Main MJ, Powell AJ, Gladwell ZM, Hick C, Sidhu HS, et al. Heterologous expression and functional analysis of rat Nav1.8 (SNS) voltage-gated sodium channels in the dorsal root ganglion neuroblastoma cell line ND7-23. Neuropharmacology. 2004;46:425–38.
31. Pertwee RG. The diverse CB1 and CB2 receptor pharmacology of three plant cannabinoids: delta9-tetrahydrocannabinol, cannabidiol and delta9-tetrahydrocannabivarin. Br J Pharmacol. 2008;153:199–215.
32. Middleton SJ, Perini I, Themistocleous AC, Weir GA, McCann K, Barry AM, et al. Nav1.7 is required for normal C-low threshold mechanoreceptor function in humans and mice. Brain. 2022;145:3637–53.
33. Shields SD, Ahn H-S, Yang Y, Han C, Seal RP, Wood JN, et al. Nav1.8 expression is not restricted to nociceptors in mouse peripheral nervous system. Pain. 2012;153:2017–30.
34. Stewart RG, Osorno T, Fujita A, Jo S, Ferraiuolo A, Carlin K, et al. Modulation of human dorsal root ganglion neuron firing by the Nav1.8 inhibitor suzetrigine. Proc Natl Acad Sci USA. 2025;122:e2503570122.
35. Vasylyev DV, Zhao P, Schulman BR, Waxman SG. Interplay of Nav1.8 and Nav1.7 channels drives neuronal hyperexcitability in neuropathic pain. J Gen Physiol. 2024;156:e202413596.
36. Dib-Hajj SD, Geha P, Waxman SG. Sodium channels in pain disorders: pathophysiology and prospects for treatment. Pain. 2017;158:S97–S107.
37. Ross HR, Napier I, Connor M. Inhibition of recombinant human T-type calcium channels by Delta9-tetrahydrocannabinol and cannabidiol. J Biol Chem. 2008;283:16124–34.
38. Gadotti VM, Huang S, Zamponi GW. The terpenes camphene and alpha-bisabolol inhibit inflammatory and neuropathic pain via Cav3.2 T-type calcium channels. Mol Brain. 2021;14:166.
39. Ahluwalia J, Urban L, Capogna M, Bevan S, Nagy I. Cannabinoid 1 receptors are expressed in nociceptive primary sensory neurons. Neuroscience. 2000;100:685–8.
40. Veress G, Meszar Z, Muszil D, Avelino A, Matesz K, Mackie K, et al. Characterisation of cannabinoid 1 receptor expression in the perikarya, and peripheral and spinal processes of primary sensory neurons. Brain Struct Funct. 2013;218:733–50.
41. Jordt S-E, Bautista DM, Chuang H, McKemy DD, Zygmunt PM, Högestätt ED, et al. Mustard oils and cannabinoids excite sensory nerve fibres through the TRP channel ANKTM1. Nature. 2004;427:260.
42. Amawi T, Nmarneh A, Noy G, Ghantous M, Niv MY, Di Pizio A, et al. Identification of the TRPA1 cannabinoid-binding site. Pharmacol Res. 2024;209:107444.
43. Cavanaugh EJ, Simkin D, Kim D. Activation of transient receptor potential A1 channels by mustard oil, tetrahydrocannabinol and Ca2+ reveals different functional channel states. Neuroscience. 2008;154:1467–76.
44. Muller C, Morales P, Reggio PH. Cannabinoid ligands targeting TRP channels. Front Mol Neurosci. 2018;11:487.
45. Goldin AL. Mechanisms of sodium channel inactivation. Curr Opin Neurobiol. 2003;13:284–90.
46. Scheuer T. Commentary: a revised view of local anesthetic action: what channel state is really stabilized? J Gen Physiol. 1999;113:3–6.
47. Bai C-X, Glaaser IW, Sawanobori T, Sunami A. Involvement of local anesthetic binding sites on IVS6 of sodium channels in fast and slow inactivation. Neurosci Lett. 2003;337:41–45.

48. Fozzard HA, Sheets MF, Hanck DA. The sodium channel as a target for local anesthetic drugs. Front Pharmacol. 2011;2:1–6.
49. Huestis MA. Human cannabinoid pharmacokinetics. Chem Biodivers. 2007;4:1770–804.
50. Garrett ER, Hunt CA. Physiochemical properties, solubility, and protein binding of delta9-tetrahydrocannabinol. J Pharm Sci. 1974;63:1056–64.
51. Cox EJ, Maharao N, Patilea-Vrana G, Unadkat JD, Rettie AE, McCune JS, et al. A marijuana-drug interaction primer: precipitants, pharmacology, and pharmacokinetics. Pharmacol Ther. 2019;201:25–38.
52. Thomas BF, Compton DR, Martin BR. Characterization of the lipophilicity of natural and synthetic analogs of delta 9-tetrahydrocannabinol and its relationship to pharmacological potency. J Pharmacol Exp Ther. 1990;255:624–30.
53. Thorne N, Auld DS, Inglese J. Apparent activity in high-throughput screening: origins of compound-dependent assay interference. Curr Opin Chem Biol. 2010;14:315–24.
54. Huestis MA, Henningfield JE, Cone EJ. Blood cannabinoids. I. Absorption of THC and formation of 11-OH-THC and THCCOOH during and after smoking marijuana. J Anal Toxicol. 1992;16:276–82.
55. Lucas CJ, Galettis P, Schneider J. The pharmacokinetics and the pharmacodynamics of cannabinoids. Br J Clin Pharmacol. 2018;84:2477–82.
56. Heuberger JAAC, Guan Z, Oyetayo O-O, Klumpers L, Morrison PD, Beumer TL, et al. Population pharmacokinetic model of THC integrates oral, intravenous, and pulmonary dosing and characterizes short- and long-term pharmacokinetics. Clin Pharmacokinet. 2015;54:209–19.
57. Kreuz DS, Axelrod J. Delta-9-tetrahydrocannabinol: localization in body fat. Science. 1973;179:391–3.
58. Huestis MA, Smith ML. Human cannabinoid pharmacokinetics and interpretation of cannabinoid concentrations in biological fluids and tissues. Marijuana and the Cannabinoids. Totowa, New Jersey, Humana Press; 2007. p. 205–35.
59. Grant KS, Petroff R, Isoherranen N, Stella N, Burbacher TM. Cannabis use during pregnancy: pharmacokinetics and effects on child development. Pharmacol Ther. 2018;182:133–51.
60. Kauert GF, Ramaekers JG, Schneider E, Moeller MR, Toennes SW. Pharmacokinetic properties of delta9-tetrahydrocannabinol in serum and oral fluid. J Anal Toxicol. 2007;31:288–93.
61. Marsot A, Audebert C, Attolini L, Lacarelle B, Micallef J, Blin O. Comparison of cannabinoid concentrations in plasma, oral fluid and urine in occasional cannabis smokers after smoking cannabis cigarette. J Pharm Pharm Sci. 2016;19:411–22.
62. Schwilke EW, Schwope DM, Karschner EL, Lowe RH, Darwin WD, Kelly DL, et al. Delta9-tetrahydrocannabinol (THC), 11-hydroxy-THC, and 11-nor-9-carboxy-THC plasma pharmacokinetics during and after continuous high-dose oral THC. Clin Chem. 2009;55:2180–9.
63. Morales P, Hurst DP, Reggio PH. Molecular targets of the phytocannabinoids: a complex picture. Prog Chem Org Nat Prod. 2017;103:103–31.

AUTHOR CONTRIBUTIONS

Conceptualization, AB and AP; Investigation, YM and AI; Formal Analysis, YM, AB, and AP; Writing—Original Draft, YM, AB, and AP; Funding Acquisition, AB and AP; Supervision, AB and AP.

FUNDING

This work was funded by: The Israel Science Foundation—Individual Research Grant 2136/20 & 2202/25 (AP), The Israel Science Foundation—Individual Research Grant 1202/23 (AB), and The Israel Science Foundation—Biomedical Sciences 2869/25 (AB). Israel Cancer Research Fund (ICRF)—The Brause Family Initiative for Quality of Life 22-402-QOL (AB, AP). Cecile and Seymour Alpert Chair in Pain Research (AB) and Jacob Gitlin Chair in Physiology (AP). Open access funding provided by Hebrew University of Jerusalem.

COMPETING INTERESTS

The authors declare no competing interests.

ADDITIONAL INFORMATION

Supplementary information The online version contains supplementary material available at https://doi.org/10.1038/s41386-026-02355-9.

Correspondence and requests for materials should be addressed to Alexander M. Binshtok or Avi Priel.